Integrated germanium optical interconnects on silicon substrates

Papichaya Chaisakul[1], Delphine Marris-Morini[1]*, Jacopo Frigerio[2], Daniel Chrastina[2], Mohamed-Said Rouifed[1], Stefano Cecchi[2], Paul Crozat[1], Giovanni Isella[2] and Laurent Vivien[1]

The integration of optical data communication with electrical data computing via Si complementary metal–oxide–semiconductor (CMOS) technology could revolutionize information technology. Indeed, chip-scale optical interconnection has been identified as possibly the most viable solution to overcome the imminent performance limit of CMOS integrated circuits due to the short distance (board-to-board, chip-to-chip, core-to-core, core-to-memory) data communication bottleneck[1–3], and both hybrid and monolithic Si photonics have been heavily investigated[3–7]. Monolithic Ge-based photonics has been regarded as one of the most promising options to realize active optical functionalities in Si CMOS-compatible photonic circuitry. Despite being an indirect-gap semiconductor, the direct-gap optical properties of Ge have been extensively explored. Ge-based devices (either bulk Ge or Ge quantum wells, QWs) have shown efficient optical modulation and photodetection within the telecommunication wavelength range in terms of both energy consumption and bandwidth[7–23]. So far, integration of active Ge optoelectronics with passive optical circuitry has been based mostly on the commonly used photonic silicon-on-insulator (SOI) waveguides[9–18]. The high refractive index contrast between the CMOS-compatible materials Si and SiO_2 is expected to open a route towards large-scale photonic–electronic integration. However, this widely investigated approach can be problematic for chip-scale integration of optical interconnection. Looking at microelectronic chips, it has to be considered that more than 90% of commercialized Si CMOS chips are based on bulk Si substrates as the cost of SOI wafers is considered prohibitive for high-volume markets such as personal computers[24] (download.intel.com/newsroom/kits/22nm/pdfs/22nm-Details_Presentation.pdf). Even for microelectronic applications using SOI substrates, the requirements of extremely thin SOI ($\ll$100 nm buried oxide) are not compatible with those of photonics (buried oxide >1 μm; top silicon >200 nm). Realizing both Ge and Si photonics and Si electronics on a thick SOI substrate is possible[25,26], but can lead to a significant degradation of the electronic performance in terms of heat dissipation and device reliability[27]. Accordingly, this approach is made available only for server-level data communication (www.luxtera.com, www.kotura.com). In addition, although the local formation of a thick oxide layer on Si is possible, it is likely to require radical changes in the front-end of line (FEOL) Si CMOS process design[28], which would prohibit its practical adoption. Wafer bonding of two separately prepared photonic and electronic chips has been demonstrated[29,30]. Nevertheless, this non-monolithic approach faces challenges in terms of the parasitic capacitance between the driving electronics and the photonics, which could severely offset the underlying benefits of implementing optical instead of copper interconnections in terms of bandwidth and energy efficiency[30]. It is also worth noting that monolithic integration of Ge crystals on amorphous silicon (a-Si) into the back-end of line (BEOL) process is also under investigation[31] at temperatures $\leq$450 °C, the upper limit for any process after FEOL. However, an active photonic device has not yet been demonstrated based on this approach. In summary, electronic–photonic integration has so far been hindered by compromised performance, increased complexity and the cost of modifying Si CMOS technology. A new concept of photonic integration that could allow the realization of optical circuitry alongside Si CMOS electronics on bulk Si wafer, while respecting its temperature constraints, is proposed and experimentally validated in this work.

In this Article, we present a new approach to monolithically integrate low-voltage, broadband photonic interconnections on a bulk Si platform. We propose and experimentally prove that Ge-rich $Si_{1-x}Ge_x$ with a well-selected x concentration (0.84 in the following demonstration) can be used as both a compact and low-loss waveguide platform and a virtual substrate (VS) on which low-temperature ($\leq$450 °C) epitaxial growth of well-chosen Ge QWs can be performed (Fig. 1). The Ge concentration x of the $Si_{1-x}Ge_x$ layer is designed to be low enough to avoid significant $Si_{1-x}Ge_x$ indirect-gap absorption[32] at the wavelength at which the Ge/SiGe MQW stack exhibits the strong quantum-confined Stark effect (QCSE). At the same time, the $Si_{1-x}Ge_x$ layer (VS) x concentration needs to be high enough to ensure a sufficiently small lattice mismatch with the Ge/SiGe MQWs, so that dislocations are not introduced from strain relaxation of the MQW stack. Usually, the

[1] Institut d'Electronique Fondamentale, Université Paris-Sud, CNRS UMR 8622, Bâtiment 220, 91405 Orsay Cedex, France, [2]L-NESS, Dipartimento di Fisica del Politecnico di Milano, Polo di Como, Via Anzani 42, I-22100 Como, Italy. *e-mail: delphine.morini@u-psud.fr

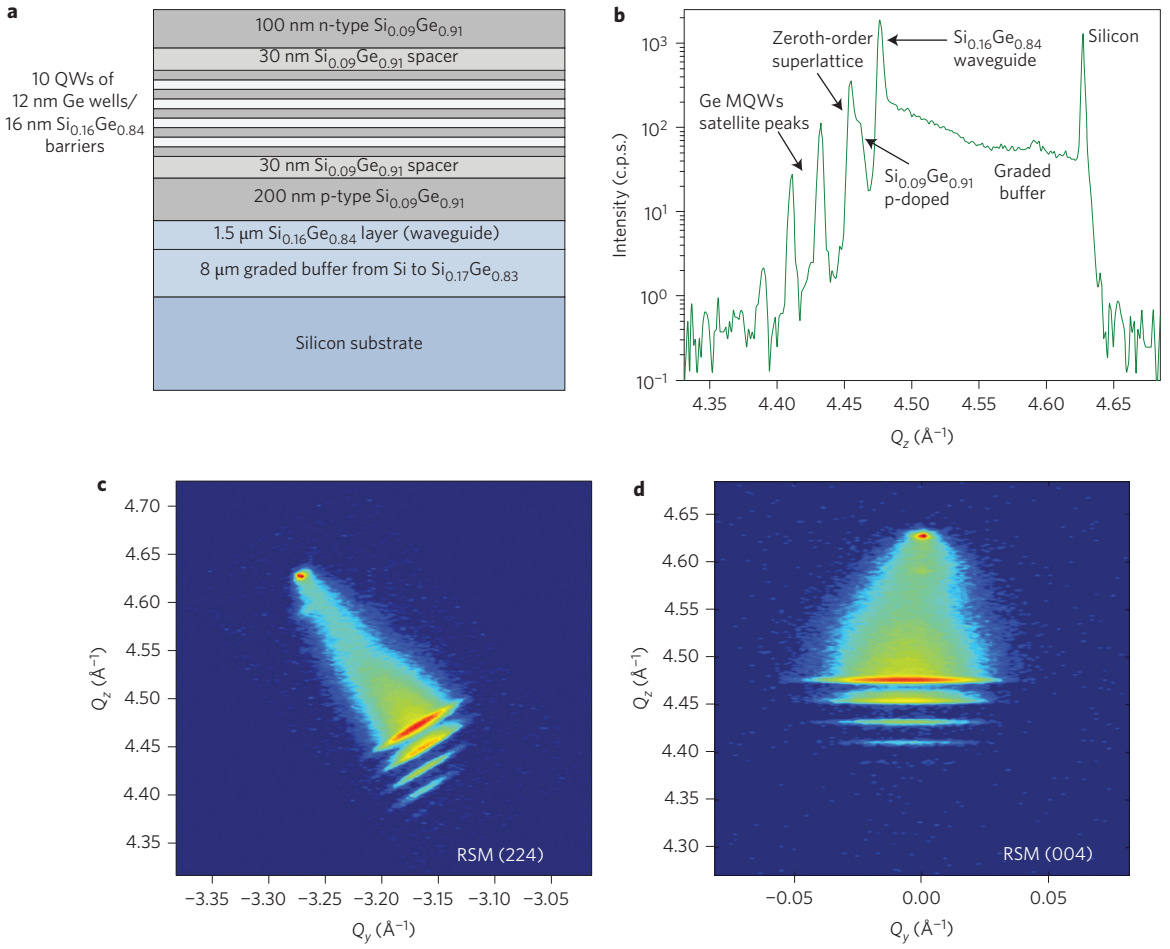

Figure 1 | Epitaxial growth and its HR-XRD characterization a, Schematic of the Ge/SiGe MQWs and SiGe waveguide stacks grown on a Si substrate via a graded buffer by LEPECVD. **b**, X-ray diffraction ω-2θ scan along the [001] direction through the (004) Bragg peak. The intensity is integrated along a Q_y range of 0.025 Å^{-1}. **c**,**d**, RSMs in the vicinity of the (224) (**c**) and (004) (**d**) reflections. Q_y and Q_z indicate longitudinal and perpendicular components of the momentum transfer, respectively.

Ge content of the VS is chosen to be equal to the average Ge content of the MQW stack so that the MQW stack is 'strain-balanced'[7,8,16,17,19,21,22], but the absorption in the $Si_{1-x}Ge_x$ VS layer at this high Ge content would lead to unacceptable waveguide optical losses at the operating wavelength of the Ge-based optoelectronic devices. Therefore, our approach allows low-loss waveguide integration of Ge-based QCSE devices on an Si substrate, which has been the crucial missing feature necessary for their practical adoption and monolithic integration with Si technology. Epilayer deposition was performed on a 4-inch Si wafer using fast epitaxial growth by low-energy plasma-enhanced chemical vapour deposition (LEPECVD)[33,34]. The procedure is described in the Methods. A sketch of the layer stack is presented in Fig. 1a.

High-resolution X-ray diffraction characterization

A (004) $\omega - 2\theta$ scan and the reciprocal space mapping (RSM) around the (224) and (004) reflections were obtained using a PANalytical X'Pert PRO MRD diffractometer, and confirmed the good crystal quality of the heterostructures. From the (004) $\omega - 2\theta$ scan in Fig. 1b, the Si substrate (004) peak is clearly visible. The zeroth-order peak gives an average Ge composition of the Ge/SiGe MQWs of 92%. Sharp higher-order satellite peaks are observed and, from the peak spacing, a superlattice period of 28 nm is deduced, which corresponds to 12-nm-thick Ge QW and 16-nm-thick $Si_{0.16}Ge_{0.84}$ barriers based on the nominal growth parameters. The peak positions of the waveguide and p-doped layers indicate Ge fractions (with respect to the Si reflection peak) of 84% ($Si_{0.16}Ge_{0.84}$) and 91% ($Si_{0.09}Ge_{0.91}$), respectively. The (224) and (004) RSMs in Fig. 1c and d confirm the good quality of the superlattice. Due to the compositional mismatch between the Ge/$Si_{0.15}Ge_{0.84}$ MQWs and the $Si_{0.16}Ge_{0.84}$ waveguide, their corresponding peaks on the (224) RSM do not share the same longitudinal components of the momentum transfer (Q_y) as in strain-balanced lattice match heterostructures[35]. Despite the compositional mismatch between the $Si_{0.16}Ge_{0.84}$ waveguide layer and the Ge/$Si_{0.15}Ge_{0.84}$ MQWs, and the associated slight degree of strain relaxation, the MQW stack maintains a high crystalline quality.

Demonstrations of Ge optical interconnects

To demonstrate the use of these heterostructures as an effective monolithic photonic interconnect, three kinds of photonic device were lithographically fabricated on the same chip with the same process flows: (1) $Si_{0.16}Ge_{0.84}$ waveguides with different lengths (Fig. 2a), (2) a stand-alone Ge/$Si_{0.16}Ge_{0.84}$ MQW p–i–n diode (Fig. 2b), and (3) a photonic interconnection based on a Ge/$Si_{0.16}Ge_{0.84}$ MQW optical modulator and photodetector integrated with a $Si_{0.16}Ge_{0.84}$ waveguide (Fig. 2c). Devices (1) and (2) are used to prove the feasibility of the $Si_{0.16}Ge_{0.84}$ layer as a low-loss waveguide at the wavelength region in which a strong electro-absorption effect is obtained from the Ge/$Si_{0.16}Ge_{0.84}$ MQWs. Devices (3) demonstrate low-voltage and broadband operation of the photonic interconnects. A top-down approach, as

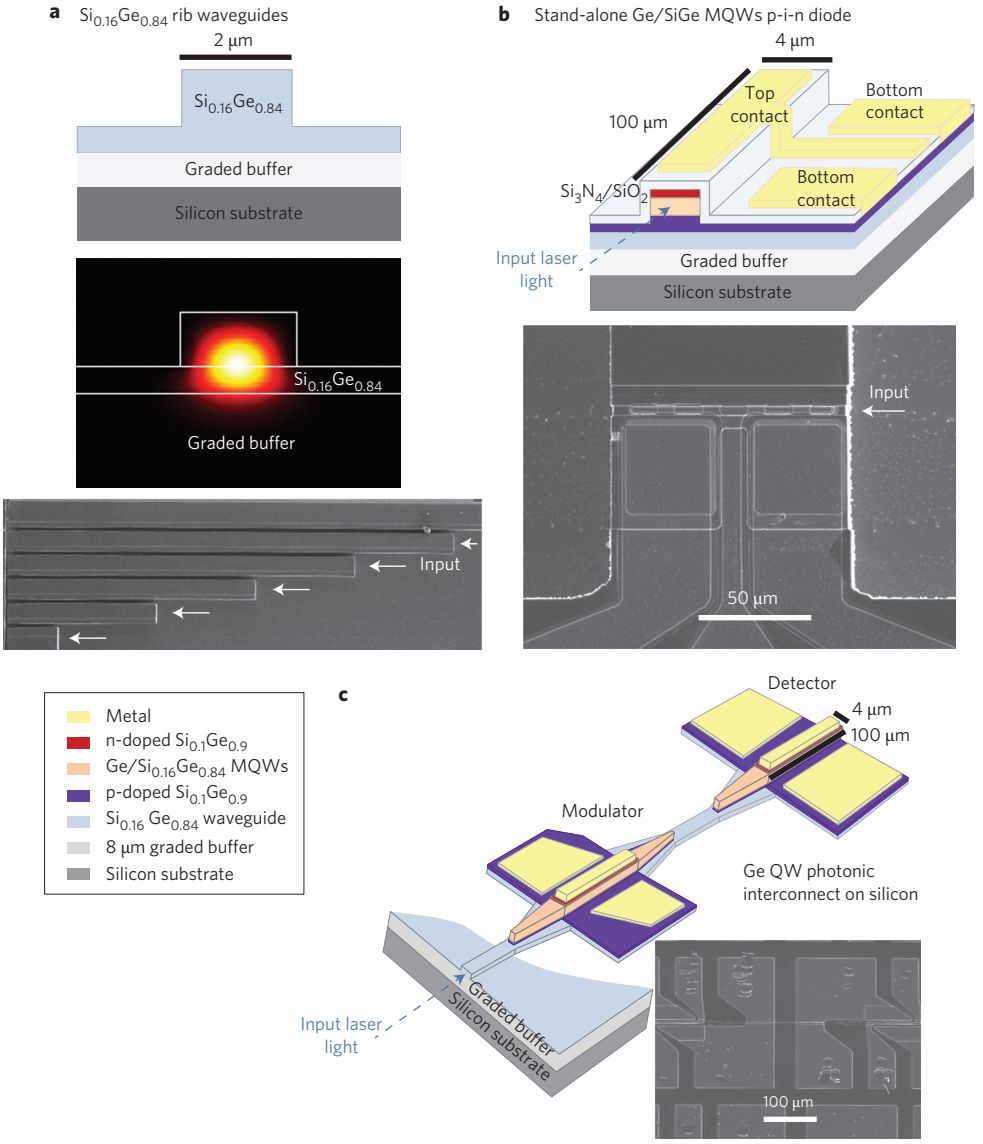

Figure 2 | Schematic and scanning electron microscopy (SEM) views of the three kinds of photonic device fabricated on the same chip and with the same process flows. a, $Si_{0.16}Ge_{0.84}$ rib waveguides (2 μm wide, 1.5 μm high and 1 μm etched) of different lengths for propagation loss characterization. Lower inset: film mode-matching simulation showing the single-mode condition of the TE-polarized guided light. **b**, A stand-alone 4-μm-wide and 100-μm-long Ge/SiGe MQW p-i-n diode. **c**, Fabricated photonic interconnect consisting of a passive $Si_{0.16}Ge_{0.84}$ waveguide and active $Ge/Si_{0.16}Ge_{0.84}$ MQW optical modulator and photodetector (the taper section is 55 μm long).

described in the Methods, was used to realize the integrated photonic interconnection by means of different etching steps, as the passive $Si_{0.16}Ge_{0.84}$ waveguide layer was already embedded under the $Ge/Si_{0.16}Ge_{0.84}$ MQW optical modulator and photodetector.

$Si_{0.16}Ge_{0.84}$ waveguide

$Si_{0.16}Ge_{0.84}$ rib waveguides (2 μm wide, 1.5 μm high and 1 μm etched) were fabricated as shown in Fig. 2a. Simulations using a film mode-matching complex solver assuming a linear variation of refractive index in the graded buffer, as in the middle inset of Fig. 2a, give an effective index of 4.11. The propagation loss was measured using a cut-back method on a set of waveguides 750, 1,250, 1,750, 2,250 and 2,750 μm long. Optical transmission measurements were performed on each waveguide in the wavelength range 1,340–1,540 nm. By plotting a graph of the transmitted optical power against waveguide (Fig. 3a), the propagation losses of the fabricated $Si_{0.16}Ge_{0.84}$ waveguide were deduced for the wavelength of interest. As shown in Fig. 3b, propagation losses of less than 5 dB cm^{-1} and 2 dB cm^{-1} can be obtained at wavelengths longer than 1,410 nm and 1,440 nm, respectively. These values are consistent with previous works on bulk SiGe alloys[32]. Although the refractive index contrast between the waveguide core and the graded buffer is low, strong light confinement and tight bend radius could be obtained in future works by etching through the waveguide core at the bent section[36,37].

A stand-alone Ge/SiGe MQW device

The electro-optic properties of $Ge/Si_{0.16}Ge_{0.84}$ MQWs (with a mean Ge content of 92%) directly grown on top of the $Si_{0.16}Ge_{0.84}$ layer (Fig. 2b) are presented in Fig. 4a. From photocurrent spectroscopy, at 0 V bias, a clear exciton peak at room temperature is observed around 0.888 eV, which can be attributed to the transition between the first valence band heavy hole level (HH1) and the first conduction band state at Γ (cΓ1), in good agreement with the transition energy obtained by means of an eight-band **k·p** calculation (www.nextnano.de/nextnano3). By increasing the reverse bias

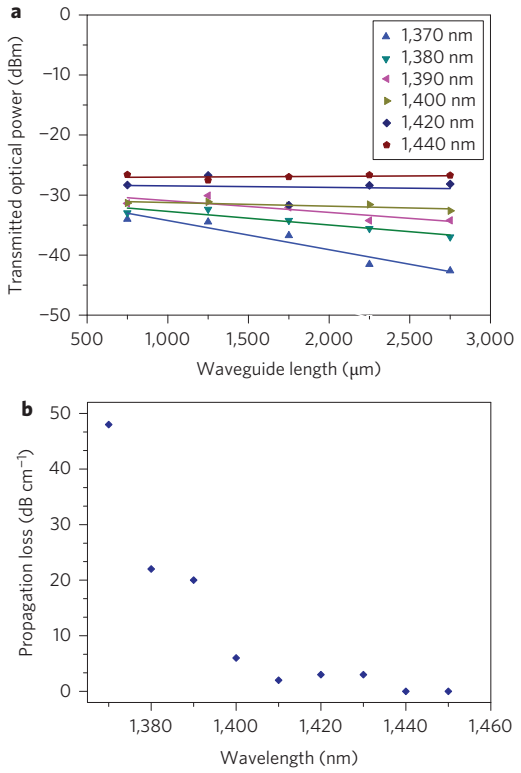

Figure 3 | Characterizations of the $Si_{0.16}Ge_{0.84}$ waveguides. a, Measured transmitted optical power versus waveguide length at different wavelengths. **b**, Propagation loss of the fabricated $Si_{0.16}Ge_{0.84}$ waveguides (Fig. 2a) obtained via a cut-back method.

voltage, two main characteristics of the QCSE are obtained: the Stark (red) shift of the absorption spectra and the reduction of the exciton-related absorption peak due to the reduction of the overlap between the electron and hole wavefunctions. Significantly, a large absorption variation is obtained at wavelengths longer than 1,420 nm, so the underlying $Si_{0.16}Ge_{0.84}$ layer can act as a low-loss waveguide as previously shown (Fig. 3). This confirms that, within a given range of compositional mismatch, it is possible to design low-optical-loss Ge-rich $Si_{1-x}Ge_x$ VS with appropriate Ge concentration x, on which high-quality Ge-based optoelectronic structures can be directly grown at low temperature without the use of sophisticated annealing procedures. It is worth noting that such a Ge/SiGe MQW p–i–n diode can be used as a modulator or a photodiode, depending on the operation mode. This, together with the use of high-Ge-content SiGe waveguides, is a key point for the realization of an optical interconnect scheme relying on a single material platform. The Ge/$Si_{0.16}Ge_{0.84}$ MQWs, when used as a photodiode, exhibit optical responsivities of 0.3–0.6 A W^{-1} (Fig. 4a), and when used as a modulator, an extinction ratio of 3.5–4 dB with 2–3 dB loss over 20 nm spectral ranges from 1,430 to 1,450 nm between bias voltages of 0 and 3 V (Fig. 4b). It has been mentioned by Schaevitz *et al.* that an optical modulator with 5 dB extinction ratio and 3 dB insertion loss could be considered suitable for chip-scale communication[38]. The wavelength separation of ~5 nm between each transmission peak is consistent with the Fabry–Pérot resonance between the input and the output facets of the waveguide. Additionally, it is worth mentioning that the responsivity and modulation performance of the prototype based on the lattice-mismatched epitaxial Ge/SiGe MQWs in this work show no degradation compared to our previous works using conventional Ge/SiGe MQWs with the same average Ge content as the VS[21,39]. Any performance differences between this work and our previous works are mainly due to the lower number of QWs (10 QWs) used here, instead of 20 QWs previously. Figure 4c,d reports on the detection and modulation bandwidths. Cutoff frequencies of 4 GHz and 6.3 GHz are obtained for detector and modulator, respectively. The measured bandwidth is RC limited. We have estimated a relatively large device capacitance of 200 fF from this $4 \times 100\ \mu m^2$ prototype with 350-nm-thick intrinsic regions. Both d.c. and radiofrequency (RF) performance can be obviously improved by optimizing the device dimensions and layer thicknesses to obtain a better overlap between the optical field, active Ge/SiGe materials and bias electric field, as discussed by Schaevitz and co-authors[38]. The measured detection bandwidth is lower than the modulation bandwidth because the photocurrent from the detector was measured with an additional 50 Ω serial resistance due to the input impedance of the network analyser, resulting in a larger RC time constant. Regarding the prospect of C-band operation, as shown in Fig. 4a,b the Ge/$Si_{0.16}Ge_{0.84}$ MQWs exhibit a noticeable modulation at 1,540 nm at a reverse bias of 5 V (14.2×10^4 V cm^{-1}). In MQWs it is possible to apply electric fields higher than the breakdown field of the bulk material, as the hole and electron wavefunctions are displaced from the bandedges due to quantum confinement, resulting in increased ionization energy[40]. For low-bias operation, it is predicted by Lever *et al.*[41] and Schaevitz *et al.*[38] that compressive strain in the Ge QWs can be reduced to allow efficient modulation at 1.55 μm by increasing the average Ge composition in the MQWs to 95–97%. For our SiGe waveguide integration we could use, for example, $Si_{0.1}Ge_{0.9}$ (instead of the $Si_{0.16}Ge_{0.84}$ used in this Article) as a platform to grow such MQWs. Based on the results obtained here regarding the tolerable level of lattice mismatch and the $Si_{0.1}Ge_{0.9}$ absorption coefficient (<1 cm^{-1}) at 1.55 μm reported in the literature[32], the SiGe waveguide approach could also be used to define an optical interconnection at 1.55 μm.

Integrated Ge modulator and photodetector

The *I–V* characteristics without illumination (dark current) of the Ge/SiGe MQW devices integrated on the $Si_{0.16}Ge_{0.84}$ waveguide (Fig. 2c) are reported in Fig. 5a for ten devices fabricated on the same chip. Almost all the prototypes exhibit excellent diode rectifying behaviour up to a reverse bias of 6 V. The reverse current is five orders of magnitude lower than the forward current, confirming the good crystal quality of the MQWs, as previously observed from the high-resolution X-ray diffraction (HR-XRD) measurements, and highly competitive with state-of-the-art III–V photonic devices bonded on Si[42]. With illumination from the input $Si_{0.16}Ge_{0.84}$ waveguide, as indicated in Fig. 2c, the first and second MQW devices on the light path are used as a modulator and a photodetector, respectively. The *I–V* characteristics obtained when the same bias voltages are applied to both optical modulator and photodetector are reported in Fig. 5b using 3 mW input light at a wavelength of 1,440 nm. The photocurrent level in the detector is lower than that at the optical modulator by a factor of only three, and the devices are of the same size. This indicates that the optical insertion loss of our Ge/SiGe MQW device integrated on a $Si_{0.16}Ge_{0.84}$ waveguide, including both in- and outcoupling and the Ge/SiGe MQW background absorption loss, is less than 5 dB. This is even slightly better than that reported for high-performance low-loss III–V components bonded on Si[43]. At a reverse bias lower than 3 V, the photocurrents at the optical modulator and photodetector are more than three orders of magnitude higher than the dark currents. Figure 5c shows the *I–V* characteristic of the photodetector for different bias voltages applied to the modulator at 1,440 nm. Modulations of 5 and 10 μA between the lower level ('0') and the upper level ('1') of the optical signal are obtained at the photodetector using a 1 V swing (between 1 and 2 V) and 3 V swing (between 0 and 3 V) at the optical modulator,

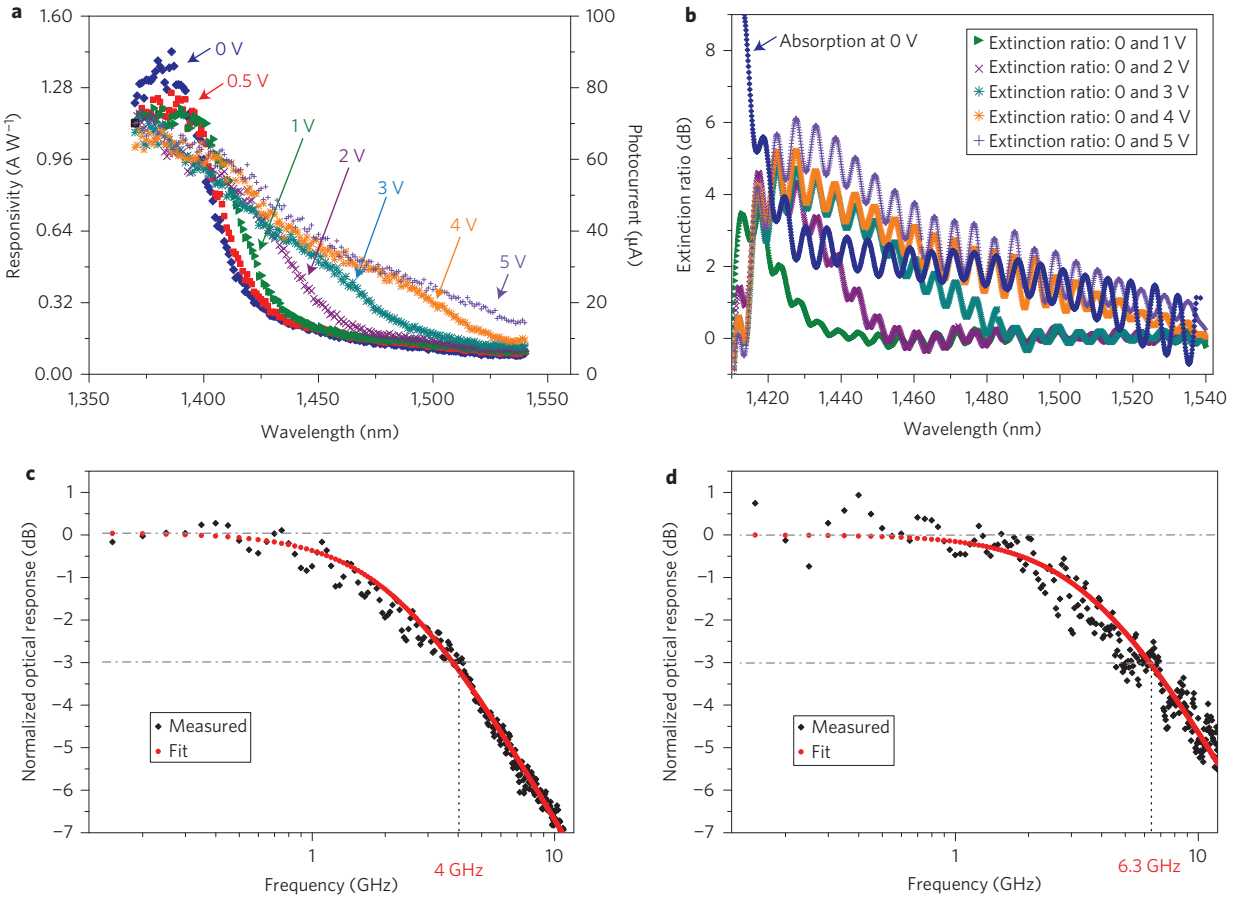

Figure 4 | Characterizations of the stand-alone Ge/$Si_{0.16}Ge_{0.84}$ MQWs modulator and photodetector. a,**b**, Photocurrent spectra (**a**) and extinction ratio (**b**) versus absorption loss obtained from transmission measurements at different bias voltages of the 4-μm-wide and 100-μm-long Ge/$Si_{0.16}Ge_{0.84}$ MQWs (Fig. 2b) grown on top of the $Si_{0.16}Ge_{0.84}$ layer. Strong QCSE is obtained at wavelengths longer than 1,420 nm, where the underlying $Si_{0.16}Ge_{0.84}$ layer can act as a low-loss waveguide, as shown in Fig. 3. **c**,**d**, Optical detection (**c**) and optical modulation bandwidths (**d**) of the Ge/$Si_{0.16}Ge_{0.84}$ MQWs device.

respectively. The photodetecor bias is −1 V and the dark current is 10 nA. The modulated electrical signal detected at the photodetector is three orders of magnitude larger than the dark current level, one of the main noise contributions. Moreover, an estimated shot noise value of 2.5 pA $Hz^{-1/2}$ is also sufficiently lower than the modulation amplitude[44]. These suggest that this integration scheme of Ge/SiGe MQWs on a $Si_{0.16}Ge_{0.84}$ waveguide has promising potential for low-bit-error-rate (BER) data transmission, the main determining factor of any practical data transmission system[45]. Moreover, it should be noted that the required voltage supply of 1–3 V brings this photonic interconnection prototype to the supply voltage levels used in CMOS technology. The voltage level can be lowered further by optimization of the Ge QW designs and optical overlap factor[17]. Moreover, we can see in the inset of Fig. 5c that similar performance can be obtained for a wide spectral range from 1,430 nm to 1,450 nm, indicating its potential for Tb s^{-1} data communication.

Conclusion

We have presented an experimental proof-of-concept integration of Ge-based photonic interconnection into planar optical circuitry on bulk Si. The prototype shows that a Ge-rich $Si_{1-x}Ge_x$ VS can be used as a compact and low-loss waveguide platform on which high-quality epitaxial growth of Ge-based optoelectronic devices can be directly performed at low temperature. We envision that this Ge-rich $Si_{1-x}Ge_x$ VS can be realized during the formation of Si transistor devices on the same Si substrate. Subsequently, Ge-based active devices can be produced at low temperature (<450 °C) to avoid significant modification of the standard FEOL CMOS process, creating a monolithic optical circuitry on bulk Si substrate next to Si electronics. For this proof-of-concept work, the fraction of Ge in the $Si_{1-x}Ge_x$ waveguide has to be carefully selected to satisfy two conflicting and crucial requirements: the Ge content x needs to be (1) low enough to avoid optical absorption at the working wavelength range, and (2) high enough to have a small lattice mismatch with the MQW stack to ensure high-quality direct epitaxial growth of the MQW on the waveguide layer. Clever use of the $Si_{0.16}Ge_{0.84}$ layer as both low-loss waveguide and VS maintains the high crystalline quality of the Ge/$Si_{0.15}Ge_{0.84}$ MQWs, despite the compositional mismatch. These conditions were experimentally confirmed using HR-XRD, *I*–*V* characterization, optical transmission and photocurrent measurements on the epitaxial layers and the fabricated prototypes. Moreover, photonic interconnection of a passive $Si_{0.16}Ge_{0.84}$ waveguide and optoelectronic Ge/$Si_{0.16}Ge_{0.84}$ MQWs devices including an optical modulator and a photodetector has been demonstrated, confirming the strong potential of their use for high-quality data transmission over a wide spectral range of more than 20 nm, as required for on-chip Tb s^{-1} systems. It should be noted that the practical advantages of using an on-chip optical interconnection with an off-chip optical supply for chip-scale data communication applications have been compellingly discussed by Miller[2]. Finally, besides Ge QWs, this concept opens a route towards a new strategy of integrating photonic interconnects with bulk Si CMOS microelectronics. For instance, our approach can be extended to any kind of Ge photonic device (bulk Ge/bulk SiGe) working within telecommunication wavelengths given that a

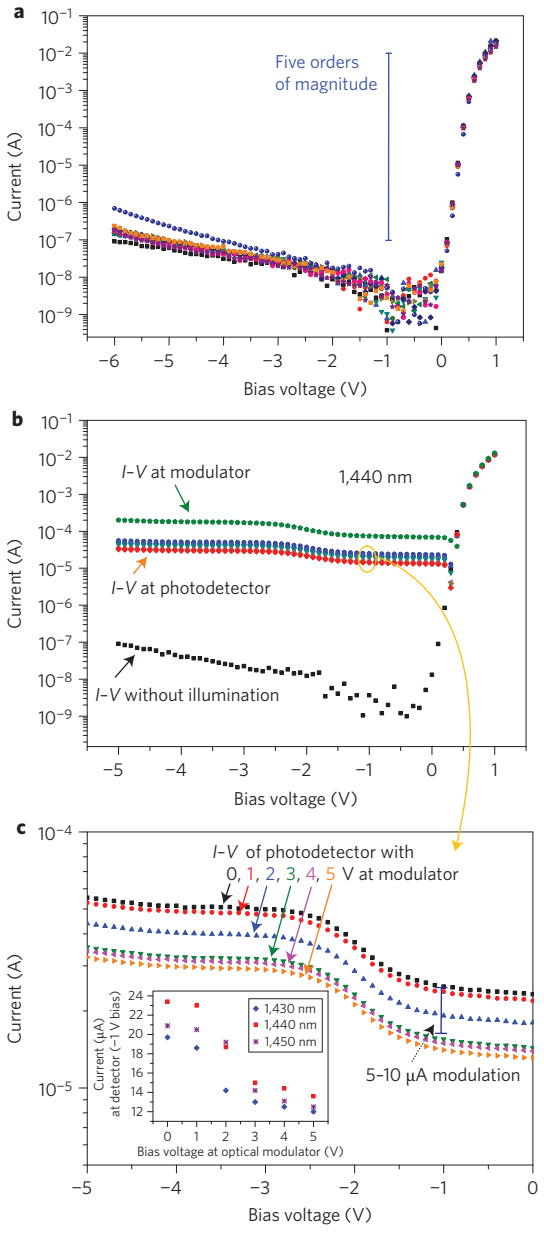

Figure 5 | Characterizations of the integrated optical interconnects of a passive $Si_{0.16}Ge_{0.84}$ waveguide and active Ge/$Si_{0.16}Ge_{0.84}$ MQW modulator and photodetector. a, *I–V* characteristics without illumination (dark current) of the Ge/SiGe MQWs integrated on a $Si_{0.16}Ge_{0.84}$ waveguide (Fig. 2c) for ten randomly selected devices. **b**, *I–V* characteristics of the fabricated photonic interconnect (Fig. 2c), when the first device is used as an optical modulator and the second device as a photodetector. **c**, Photocurrents at the photodetector with different reverse-bias voltages at the optical modulator; 5 μA and 10 μA modulations are obtained at the photodetector with 1 V swing (between 1 and 2 V) and 3 V swing (between 0 and 3 V) applied at the optical modulator. The photodetector bias is −1 V and the dark current is 10 nA. Inset: similar performance can be obtained for a wide spectral range from 1,430 nm to 1,450 nm.

suitable Ge content x for the Ge-rich $Si_{1-x}Ge_x$ waveguide layer is selected.

Methods

Epitaxial growth and device fabrications. The Ge/SiGe MQWs were grown by LEPECVD at 425 °C (ref. 33) on a 100 mm p-Si(001) substrate with a resistivity of 1–10 Ωcm. Before heteroepitaxy, the native oxide was removed by dipping the substrate in aqueous HF solution (HF:H_2O 1:10) for 30 s. The first part of the structure consisted of an 8-μm-thick Si_{1-y} Ge_y graded buffer, deposited at a rate of 5–10 nm s^{-1}, in which the Ge concentration y is linearly increased from 0% to 83%. A 1.5-μm-thick $Si_{0.16}Ge_{0.84}$ layer was deposited to be used as a waveguide. Subsequently, the Ge MQW stack with a mean Ge concentration of 92% was deposited. A 200 nm B-doped (~1×10^{19} cm^{-3}) $Si_{0.09}Ge_{0.91}$ layer was deposited to form the p-type contact region, followed by a 30 nm $Si_{0.09}Ge_{0.91}$ spacer. The MQW structure consisted of ten periods of 12-nm-thick Ge QWs and 16-nm-thick $Si_{0.16}Ge_{0.84}$ barriers grown at a rate of 1 nm s^{-1}. Finally, a 30 nm $Si_{0.11}Ge_{0.91}$ layer spacer and 100 nm P-doped (~1×10^{19} cm^{-3}) $Si_{0.09}Ge_{0.91}$ layer were deposited. A cross-section of the device is shown in Fig. 1a. The active Ge MQW optical modulator and photodetector and passive SiGe waveguide were fabricated simultaneously. The fabrication steps consisted of five ultraviolet lithography steps of (1) mesa etching down to the p-doped layer, (2) removal of the remaining p-doped layer on the underlying $Si_{0.16}Ge_{0.84}$ layer and of the n-doped layer on the taper section of the mesa, (3) $Si_{0.16}Ge_{0.84}$ waveguide patterning, (4) Si_3N_4/SiO_2 insulation layer deposition by PECVD and patterning of contact vias by dry and wet etching, and (5) metallization of Al. The stand-alone $Si_{0.16}Ge_{0.84}$ waveguides and Ge/SiGe MQWs p–i–n diodes (Fig. 2a,b) were also realized on the same chip during these fabrication processes.

Optical transmission and photocurrent measurements. For all characterizations, light from a tunable laser (TUNICS, Yenista Optics) was butt-coupled into the optical tested devices using a lensed fibre. A polarizer was used between the light source and the device to selectively inject light with the electric field parallel to the Ge QW plane (TE polarization). For optical transmission measurements of $Si_{0.16}Ge_{0.84}$ waveguides, transmitted light was coupled into a photodetector by an objective system. The spectra were swept simultaneously from 1,330 nm to 1,540 nm (All-Band Optical Component Tester MT9820A, Anritsu) with a spectral resolution of less than 0.1 nm. For the photocurrent spectra measurement of a stand-alone Ge/SiGe MQW p–i–n diode, lock-in detection was used to record the wavelength-dependent photocurrent signal at various bias voltages with a spectral resolution of 1 nm. For this purpose, a chopper and lock-in amplifier were used to modulate the light intensity at 1 kHz and measure the photocurrent spectra. For characterization of the photonic interconnection of a passive $Si_{0.16}Ge_{0.84}$ waveguide and active Ge/$Si_{0.16}Ge_{0.84}$ MQW 100-μm-long optical modulator and photodetector, the required reverse-bias voltage on each of the two active devices was applied by a separate voltage source, which also recorded the values of the corresponding photogenerated current at each bias voltage and input light wavelength. A computer was connected to the voltage source via a GPIB interface, allowing the simultaneous acquisition of the *I–V* characteristics.

RF measurements. The frequency response of the Ge/SiGe MQW photodiode was measured using an Agilent 86030A lightwave component analyser (LCA). An external light source at 1,540 nm was modulated by a lithium niobate modulator driven by the LCA and sent to the photodetector. An RF probe was used to reverse-bias the device at −5 V and collect the photogenerated carriers. As a modulator, the frequency response was also evaluated at 1,540 nm. An a.c. electrical signal generated by the Agilent 86030A opto-RF vector network analyser coupled with a d.c. bias-tee was used to drive the modulator. The modulated optical signal was coupled back to the opto-RF vector network analyser by objective lenses. The normalized optical response was measured at a d.c. reverse bias of −5 V.

Received 25 October 2013; accepted 6 March 2014;
published online 11 May 2014

References

1. Kirchain, R. & Kimerling, L. A roadmap for nanophotonics. *Nature Photon.* **1,** 303–305 (2007).
2. Miller, D. A. B. Device requirements for optical interconnects to silicon chips. *Proc. IEEE* **97,** 1166–1185 (2009).
3. Wada, K. A new approach of electronics and photonics convergence on Si CMOS platform: how to reduce device diversity of photonics for integration. *Adv. Opt. Technol.* **2008,** 807457 (2008).
4. Kuo, Y., Chen, H.-W. & Bowers, J. E. High speed hybrid silicon evanescent electroabsorption modulator. *Opt. Express* **16,** 9936–9941 (2008).
5. Fang, A. W. *et al.* Electrically pumped hybrid AlGaInAs-silicon evanescent laser. *Opt. Express* **14,** 9203–9210 (2006).
6. Van Campenhout, J. *et al.* Electrically pumped InP-based microdisk lasers integrated with a nanophotonic silicon-on-insulator waveguide circuit. *Opt. Express* **15,** 6744–6749 (2007).
7. Kuo, Y.-H. *et al.* Strong quantum-confined Stark effect in germanium quantum-well structures on silicon. *Nature* **437,** 1334–1336 (2005).
8. Chaisakul, P. *et al.* Quantum-confined Stark effect measurements in Ge/SiGe quantum-well structures. *Opt. Lett.* **35,** 2913–2915 (2010).
9. Assefa, S. *et al.* CMOS-integrated high-speed MSM germanium waveguide photodetector. *Opt. Express* **18,** 4986–4999 (2010).
10. Liu, J. *et al.* Waveguide-integrated, ultralow-energy GeSi electro-absorption modulators. *Nature Photon.* **2,** 433–437 (2008).

11. Feng, D. *et al.* High speed GeSi electro-absorption modulator at 1550 nm wavelength on SOI waveguide. *Opt. Express* **20,** 22224–22232 (2012).
12. Feng, D. *et al.* High-speed Ge photodetector monolithically integrated with large cross-section silicon-on-insulator waveguide. *Appl. Phys. Lett.* **95,** 261105 (2009).
13. Lim, A. E. J. *et al.* Novel evanescent-coupled germanium electro-absorption modulator featuring monolithic integration with germanium p–i–n photodetector. *Opt. Express* **19,** 5040–5046 (2011).
14. Vivien, L. *et al.* Zero-bias 40Gbit/s germanium waveguide photodetector on silicon. *Opt. Express* **20,** 1096–1101 (2012).
15. DeRose, C. T. *et al.* Ultra compact 45 GHz CMOS compatible germanium waveguide photodiode with low dark current. *Opt. Express* **19,** 24897–24904 (2011).
16. Ren, S. *et al.* Ge/SiGe quantum well waveguide modulator monolithically integrated with SOI waveguides. *IEEE Photon. Technol. Lett.* **24,** 461–463 (2012).
17. Edwards, E. H. *et al.* Low-voltage broad-band electroabsorption from thin Ge/SiGe quantum wells epitaxially grown on silicon. *Opt. Express* **21,** 867–876 (2013).
18. Park, S. *et al.* Monolithic integration and synchronous operation of germanium photodetectors and silicon variable optical attenuators. *Opt. Express* **18,** 8412–8421 (2010).
19. Ren, S., Rong, Y., Kamins, T. I., Harris, J. S. & Miller, D. A. B. Selective epitaxial growth of $Ge/Si_{0.15}Ge_{0.85}$ quantum wells on Si substrate using reduced pressure chemical vapor deposition. *Appl. Phys. Lett.* **98,** 151108 (2011).
20. Klinger, S., Berroth, M., Kaschel, M., Oehme, M. & Kasper, E. Ge-on-Si p–i–n photodiodes with a 3-dB bandwidth of 49 GHz. *IEEE Photon. Technol. Lett.* **21,** 920–922 (2009).
21. Chaisakul, P. *et al.* 23 GHz Ge/SiGe multiple quantum well electro-absorption modulator. *Opt. Express* **20,** 3219–3224 (2012).
22. Chaisakul, P. *et al.* Ge/SiGe multiple quantum well photodiode with 30 GHz bandwidth. *Appl. Phys. Lett.* **98,** 131112 (2011).
23. Luan, H.-C. *et al.* High-quality Ge epilayers on Si with low threading-dislocation densities. *Appl. Phys. Lett.* **75,** 2909–2911 (1999).
24. Orcutt, J. S. *et al.* Nanophotonic integration in state-of-the-art CMOS foundries. *Opt. Express* **19,** 2335–2346 (2011).
25. Pinguet, T., Analui, B., Masini, G., Sadagopan, V. & Gloeckner, S. 40-Gbps monolithically integrated transceivers in CMOS photonics. *Proc. SPIE* **6898,** 689805 (2008).
26. Masini, G., Capellini, G., Witzens, J. & Gunn, C. High-speed, monolithic CMOS receivers at 1550 nm with Ge on Si waveguide photodetectors. *Proc. Laser Elect. Opt. Soc.*, 848–849 (2007).
27. Bresson, N., Cristoloveanu, S., Mazuré, C., Letertre, F. & Iwai, H. Integration of buried insulators with high thermal conductivity in SOI MOSFETs: thermal properties and short channel effects. *Solid-State Electron.* **49,** 1522–1528 (2005).
28. Sherwood-Droz, N., Gondarenko, A. & Lipson, M. Oxidized silicon-on-insulator (OxSOI) from bulk silicon: a new photonic platform. *Opt. Express* **18,** 5785–5790 (2010).
29. Pan, H. *et al.* High-speed receiver based on waveguide germanium photodetector wire-bonded to 90nm SOI CMOS amplifier. *Opt. Express* **20,** 18145–18155 (2012).
30. Zheng, X. *et al.* A sub-picojoule-per-bit CMOS photonic receiver for densely integrated systems. *Opt. Express* **18,** 204–211 (2010).
31. McComber, K. A., Duan, X., Liu, J., Michel, J. & Kimerling, L. C. Single-crystal germanium growth on amorphous silicon. *Adv. Funct. Mater.* **22,** 1049–1057 (2012).
32. Braunstein, R., Moore, A. R. & Herman, F. Intrinsic optical absorption in germanium–silicon alloys. *Phys. Rev.* **109,** 695–710 (1958).
33. Isella, G. *et al.* Low-energy plasma-enhanced chemical vapor deposition for strained Si and Ge heterostructures and devices. *Solid-State Electron.* **48,** 1317–1323 (2004).
34. Falub, C. V. *et al.* Scaling hetero-epitaxy from layers to three-dimensional crystals. *Science* **335,** 1330–1334 (2012).
35. Frigerio, J. *et al.* Electro-refractive effect in Ge/SiGe multiple quantum wells. *Appl. Phys. Lett.* **102,** 061102 (2013).
36. Spiekman, L. H. *et al.* Ultrasmall waveguide bends: the corner mirrors of the future? *IEE Proc. Optoelectron.* **142,** 61–65 (1995).
37. Akiyama, S. *et al.* Air trench waveguide bend for high density optical integration. *Proc. SPIE* **5355,** 14–21 (2004).
38. Schaevitz, R. K. *et al.* Simple electroabsorption calculator for designing 1310 nm and 1550 nm modulators using germanium quantum wells. *IEEE J. Quantum Electron.* **48,** 187–197 (2012).
39. Chaisakul, P. *et al.* 10-Gb/s Ge/SiGe multiple quantum-well waveguide photodetector. *IEEE Photon. Technol. Lett.* **23,** 1430–1432 (2011).
40. Lever, L. *et al.* Modulation of the absorption coefficient at 1.3 μm in Ge/SiGe multiple quantum well heterostructures on silicon. *Opt. Lett.* **36,** 4158–4160 (2011).
41. Lever, L., Ikonic, Z., Valavanis, A., Cooper, J. D. & Kelsall, R. W. Design of Ge-SiGe quantum-confined Stark effect electroabsorption heterostructures for CMOS compatible photonics. *J. Lightwave Technol.* **28,** 3273–3281 (2010).
42. Hofrichter, J. *et al.* A low-power high-speed InP microdisk modulator heterogeneously integrated on a SOI waveguide. *Opt. Express* **20,** 9363–9370 (2012).
43. Tang, Y. *et al.* 50 Gb/s hybrid silicon traveling-wave electroabsorption modulator. *Opt. Express* **19,** 5811–5816 (2011).
44. Harris, N. C. *et al.* Noise characterization of a waveguide-coupled MSM photodetector exceeding unity quantum efficiency. *J. Lightwave Technol.* **31,** 23–27 (2013).
45. Cassan, E., Marris-Morini, D., Rouvière, M., Vivien, L. & Laval, S. C. Comparison between electrical and optical global clock distributions for CMOS integrated circuits. *Opt. Eng.* **44,** 105402 (2005).

Acknowledgements

This research received funding from the French ANR under project GOSPEL (Direct Gap Related Optical Properties of Ge/SiGe Multiple Quantum Wells) and from the European Commission (EC) through project Green Silicon. The fabrication of the device was performed at the nano-center CTU-IEF-Minerve, which is partially funded by the 'Conseil Général de l'Essonne'. This work was partly supported by the French RENATECH network.

Author contributions

P.Ch., D.M.-M. and L.V. conceived the project. P.Ch. designed and fabricated the tested devices, conducted the experiments and performed optical simulations. P.Ch. and D.M.-M. analysed the experimental data. J.F. carried out epitaxial growth and band diagram calculations. D.C. and S.C. performed HR-XRD measurements and analysis. S.C. participated in the epitaxial growth. P.Cr. participated in device characterization. All authors contributed to manuscript preparation. D.M.-M., G.I. and L.V. supervised the project.

Additional information

Reprints and permissions information is available online at www.nature.com/reprints. Correspondence and requests for materials should be addressed to D.M.M.

Competing financial interests

The authors declare no competing financial interests.